

Quasi-analytical determination of noise-induced error limits in lidar retrieval of aerosol backscatter coefficient by the elastic, two-component algorithm

Michaël Sicard,^{1,2,*} Adolfo Comerón,¹ Francisco Rocadenbosch,^{1,2}
Alejandro Rodríguez,¹ and Constantino Muñoz¹

¹Remote Sensing Laboratory (RSLAB), Department of Signal Theory and Communications,
Universitat Politècnica de Catalunya

² Institut d'Estudis Espacials de Catalunya—Centre de Recerca de l'Aeronàutica
i de l'Espai / Universitat Politècnica de Catalunya

*msicard@tsc.upc.edu

Received 19 June 2008; revised 18 November 2008; accepted 20 November 2008;
posted 21 November 2008 (Doc. ID 97645); published 7 January 2009

The elastic, two-component algorithm is the most common inversion method for retrieving the aerosol backscatter coefficient from ground- or space-based backscatter lidar systems. A quasi-analytical formulation of the statistical error associated to the aerosol backscatter coefficient caused by the use of real, noise-corrupted lidar signals in the two-component algorithm is presented. The error expression depends on the signal-to-noise ratio along the inversion path and takes into account “instantaneous” effects, the effect of the signal-to-noise ratio at the range where the aerosol backscatter coefficient is being computed, as well as “memory” effects, namely, both the effect of the signal-to-noise ratio in the cell where the inversion is started and the cumulative effect of the noise between that cell and the actual cell where the aerosol backscatter coefficient is evaluated. An example is shown to illustrate how the “instantaneous” effect is reduced when averaging the noise-contaminated signal over a number of cells around the range where the inversion is started. © 2009 Optical Society of America

OCIS codes: 010.1100, 010.1110, 010.3640, 280.1100, 280.1350, 280.3640.

1. Introduction

While it is recognized that atmospheric aerosols have an important effect on the Earth's radiation budget, their quantitative contribution to the surface radiative forcing still has one of the largest uncertainty values among those of the different forcing factors [1]. In recent years a big effort has been devoted to reduce this uncertainty through systematic measurements by, generally speaking, *in situ* and remote sensing techniques. In this respect, lidars offer the unique capability of providing height-resolved aero-

sol measurements, which is a necessary feature to improve the assessment of the aerosol effect in the radiation balance. Aerosol lidar networks operating in a coordinated manner, and frequently associated to other *in situ* or remote sensing instrumentation, are implemented or underway to provide continental-scale four-dimensional (space–time) information on aerosol distributions (e.g., see Refs. [2,3]). It is expected that the spatial coverage is extended through existing actions to integrate the regional aerosol lidar networks into a global system [4]. At the same time, space-based lidars, like the Cloud-Aerosol Lidar and Infrared Pathfinder Satellite Observations (CALIPSO) [5,6] mission, are already providing global, albeit nonsimultaneous,

0003-6935/09/020176-07\$15.00/0
© 2009 Optical Society of America

information on aerosol and cloud distributions, and this capability will be increased with future systems (e.g., Refs. [7,8]).

In this global lidar aerosol sensing scenario of cooperation between space-based instruments and ground-based coordinated networks, data quality is a requirement for lidar measurements to have a significant effect in atmospheric models and in the retrieval of aerosol microphysical properties. Therefore, there is no doubt that ground-based, elastic, backscatter lidar systems, still the most common lidar systems used at the present time, and space-based, elastic, backscatter systems have to be fully characterized in terms of error budget. The traditional way to retrieve the aerosol backscatter coefficient from signals from such systems goes through the use of the so-called two-component algorithm [9–11]. Prior to the results from Refs. [9–11], several authors had significantly contributed to the establishment of the first solution of the elastic lidar equation known as the single-component algorithm [12–14], which was deduced from the first measurements of rain intensity, equivalent to aerosol concentration in lidar terms, by radar in 1954 [15]. The stable analytical solution (still in the single-component version) of the lidar equation was formulated for the first time in Ref. [16]. Since then, many studies have investigated the effect of both assumptions necessary to solve the two-component algorithm: the boundary value [17–21] and the extinction/backscatter ratio profile [20,22,23].

Section 2 examines the differences between the single- and two-component algorithms. Section 3 gives the quasi-analytical formulation of the statistical error provoked by noise-corrupted signals on the backscatter coefficient retrieval with the two-component algorithm. Section 4 illustrates with real data the result found in Section 3. Conclusions are presented in the last section.

2. Single-Component and Two-Component Algorithms

In the late sixties the single-component algorithm [12–14] was formulated in terms of backscatter coefficient β as a function of the range R and the received power as

$$\beta(R) = \frac{\beta_m R^2 P(R)}{R_m^2 P(R_m) + 2\beta_m \int_R^{R_m} S(z) z^2 P(z) dz}, \quad (1)$$

where $P(R)$ is the power received from range R , R_m is the range from which the inversion is started, $\beta_m = \beta(R_m)$ is the boundary condition, and $S(R) = \alpha(R)/\beta(R)$, the so-called total lidar ratio, is the ratio between the atmosphere total extinction coefficient $\alpha(R)$ and the total backscatter coefficient $\beta(R)$. Following the results from Ref. [16], Eq. (1) is a reformulation of Eq. (9) from Ref. [14] after switching the integration bounds R and R_m of the integral in the numerator, and changing the sign in front of it.

In the two-component algorithm [9–11] the effects of the molecules and of the aerosols are considered separately:

$$\beta(R) = \beta_a(R) + \beta_R(R) = \frac{\beta_m R^2 P(R) \exp\left\{2 \int_R^{R_m} [S_a(z) - 8\pi/3] \beta_R(z) dz\right\}}{R_m^2 P(R_m) + 2\beta_m \int_R^{R_m} S_a(z) z^2 P(z) \exp\left\{2 \int_z^{R_m} [S_a(x) - 8\pi/3] \beta_R(x) dx\right\} dz}, \quad (2)$$

When dealing with real, noise-corrupted lidar signals, it is important to be able to quantify the error caused, not only by the two previous assumptions, but also by the effect of noise on the used algorithm. Comerón *et al.* [24] formulated the statistical error caused by noise contaminating real-life signals on the total backscatter coefficient retrieval by the single-component algorithm. However, the single-component algorithm is not widely used in practice since it does not distinguish between molecules and aerosols. The purpose of this paper is to generalize the results from Ref. [24] and to propose a quasi-analytical formulation of the statistical error limits of the aerosol backscatter coefficient retrieval for the two-component algorithm due to noise-corrupted signals.

where $\beta_a(R)$ represents the aerosol backscatter coefficient, $\beta_R(R)$ the Rayleigh (molecular) backscatter coefficient (which can be assumed to be known), and $S_a(R) = \alpha_a(R)/\beta_a(R)$ the aerosol lidar ratio given by the ratio between the aerosol extinction coefficient $\alpha_a(R)$ and the aerosol backscatter coefficient $\beta_a(R)$. This is indeed the solution that is usually employed by the lidar community to retrieve the aerosol backscatter coefficient when dealing with ground-based backscatter elastic lidars pointing in a single direction and no Raman measurements are available. Even though the single-component solution as formulated in Eq. (1) can lead mathematically to the same results, in practice it requires the knowledge of the total lidar ratio, $S(R)$, which is harder to guess than that of aerosols and less useful in practice.

3. Retrieval in the Presence of Noise

A. General Expression

In Ref. [24] the retrieval in the presence of noise was considered for the single-component algorithm. In what follows the results are generalized for the two-component algorithm case. In a general real situation the photoreceiver output is corrupted by noise and will be proportional to

$$\hat{P}(R) = P(R) + n(R), \quad (3)$$

where $n(R)$ represents the instantaneous “power noise” affecting the measurement at range R . As in Ref. [24] it is assumed that in general $n(R)$ can be made a zero-mean process that can therefore take positive and negative values, by subtracting the bias terms from the signal at the output of the photoreceiver. The magnitude retrieved with the algorithm given by Eq. (2) is then $\hat{\beta}(R)$. By substituting Eq. (3) into the expression of $\beta(R)$, one obtains after going through some algebra

$$\begin{aligned} \hat{\beta}(R) &= \hat{\beta}_a(R) + \beta_R(R) \\ &= \left[1 + \frac{n(R)}{P(R)} \right] \frac{\beta(R)}{1 + \zeta_m(R) + \zeta_i(R)}, \end{aligned} \quad (6)$$

where

$$\begin{aligned} \zeta_m(R) &= \frac{\beta(R) R_m^2 n(R_m)}{\beta_m R^2 P(R)} \exp \left\{ 2 \int_R^{R_m} [S_a(z) \right. \\ &\quad \left. - 8\pi/3] \beta_R(z) dz \right\}, \end{aligned} \quad (7)$$

$$\begin{aligned} \zeta_i(R) &= 2\beta(R) \exp \left\{ -2 \int_R^{R_m} [S_a(z) - 8\pi/3] \beta_R(z) dz \right\} \\ &\quad \frac{\int_R^{R_m} z^2 S_a(z) n(z) \exp \left\{ 2 \int_z^{R_m} [S_a(x) - 8\pi/3] \beta_R(x) dx \right\} dz}{R^2 P(R)}. \end{aligned} \quad (8)$$

$$\begin{aligned} \frac{1}{\hat{\beta}(R)} &= \left\{ \frac{1}{\beta(R)} + \frac{1}{\beta_m} \frac{R_m^2 n(R_m)}{R^2 P(R)} \exp \left\{ -2 \int_R^{R_m} [S_a(z) - 8\pi/3] \beta_a(z) dz \right\} \right. \\ &\quad \left. + \frac{2 \int_R^{R_m} S_a(z) z^2 n(z) \exp \left\{ 2 \int_z^{R_m} [S_a(x) - 8\pi/3] \beta_R(x) dx \right\} dz}{R^2 P(R) \exp \left\{ 2 \int_R^{R_m} [S_a(z) - 8\pi/3] \beta_R(z) dz \right\}} \right\} \frac{P(R)}{P(R) + n(R)}. \end{aligned} \quad (4)$$

At this point we compare Eq. (4) with the equivalent one in the error analysis for the single-component algorithm, Eq. (4) in Ref. [24], renamed $\hat{\beta}_{sc}(R)$ in order to avoid confusion and which is repeated here for the reader’s convenience with the variable change $C(z) = 1/S(z)$:

$$\begin{aligned} \frac{1}{\hat{\beta}_{sc}(R)} &= \left[\frac{1}{\beta(R)} + \frac{1}{\beta_m} \frac{R_m^2 n(R_m)}{R^2 P(R)} \right. \\ &\quad \left. + \frac{2}{R^2 P(R)} \int_R^{R_m} S(z) z^2 n(z) dz \right] \frac{P(R)}{P(R) + n(R)}. \end{aligned} \quad (5)$$

We note that both expressions are formally identical if we take into account the correspondences stated in Table 1 between Eqs. (5) (single-component) and (4) (two-component).

With these correspondences and drawing on the results of Ref. [24], we can write in the case of the two-component inversion

B. Standard Deviation of the Noise Terms

If $n(R)$ is a zero-mean process, $n(R)/P(R)$, then $\zeta_m(R)$ and $\zeta_i(R)$ are zero-mean random variables for a given R as, for all their apparent complexity, their defining expressions, Eqs. (7) and (8), are but linear operations on $n(R)$. The standard deviation of $n(R)/P(R)$ is obviously $\sigma_n(R)/P(R)$, with $\sigma_n(R)$ being the standard deviation of $n(R)$, and clearly represents the noise-to-signal ratio at range R .

The term $\zeta_m(R)$ represents the effect of the noise in the boundary cell where the inversion is started. Calling $\sigma_{nm} = \sigma_n(R_m)$ and using a procedure parallel to that employed in Ref. [24], the standard deviation of $\zeta_m(R)$ can be cast as

$$\sigma_{\zeta_m}(R) = \frac{\sigma_{nm}}{P(R_m)} \exp \left[-2 \int_R^{R_m} S_a(z) \beta(z) dz \right], \quad (9)$$

which shows the stabilizing effect of the backward algorithm also in the effect of noise in that the exponential function will be progressively lesser than 1

Table 1. Correspondence of Terms in the Solution of $\hat{\beta}(R)$ between the Single-Component and the Two-Component Algorithms

| Single-Component Eq. (5) | Two-Component Eq. (4) |
|--------------------------|--|
| $n(R)$ | $\leftrightarrow n(R) \exp\{2 \int_R^{R_m} [S_a(z) - 8\pi/3]\beta_R(z) dz\}$ |
| $P(R)$ | $\leftrightarrow P(R) \exp\{2 \int_R^{R_m} [S_a(z) - 8\pi/3]\beta_R(z) dz\}$ |
| $S(R)$ | $\leftrightarrow S_a(R)$ |

for decreasing values of $R < R_m$. This effect, however, will be small for optically thin atmospheres.

The term $\zeta_i(R)$ corresponds to the effect of noise integrated along the retrieval path. Under the reasonable assumption that noises in different resolution cells are uncorrelated, which will occur if $\Delta\tau \geq \frac{1}{2B}$, with $\Delta\tau$ the sampling period of the acquisition system and B the photoreceiver bandwidth, we can approximate [24]

$$\langle n(z_1)n(z_2) \rangle = \sigma_n^2(z_1)\Delta R\delta(z_1 - z_2), \quad (10)$$

and reasoning along the same lines as in Ref. [24] the standard deviation of $\zeta_i(R)$ can be shown to be

$$\begin{aligned} \sigma_{\zeta_i}(R) = & \frac{2\beta(R)}{R^2P(R)} \exp\left\{-2 \int_R^{R_m} [S_a(z) - 8\pi/3]\beta_R(z) dz\right\} \\ & \times \left[\Delta R \int_R^{R_m} S_a^2(z)\sigma_n^2(z)z^4 \exp\left\{4 \int_z^{R_m} [S_a(x) - 8\pi/3]\beta_R(x) dx\right\} dz \right]^{1/2}. \end{aligned} \quad (11)$$

This equation can alternatively be written

$$\begin{aligned} \sigma_{\zeta_i}(R) = & \frac{2\beta_m}{R_m^2P(R_m)} \exp\left[-2 \int_R^{R_m} S_a(z)\beta(z) dz\right] \\ & \times \left[\Delta R \int_R^{R_m} S_a^2(z)\sigma_n^2(z)z^4 \exp\left\{4 \int_z^{R_m} [S_a(x) - 8\pi/3]\beta_R(x) dx\right\} dz \right]^{1/2}. \end{aligned} \quad (12)$$

C. Error Bounds

Calling, for the sake of notation simplicity, $\eta(R) = n(R)/P(R)$ and $\zeta(R) = \zeta_m(R) + \zeta_i(R)$, the estimated aerosol backscatter coefficient is, from Eq. (6),

$$\hat{\beta}_a(R) = \beta(R) \frac{1 + \eta(R)}{1 + \zeta(R)} - \beta_R(R). \quad (13)$$

We call

$$\frac{1 + \eta(R)}{1 + \zeta(R)} = 1 + l(R). \quad (14)$$

Note that the mean of $l(R)$ is not zero, which makes $\hat{\beta}_a(R)$ biased.

The interval $(\beta_a(R), \beta_a(R) + l_u\beta(R))$ in which $\hat{\beta}_a(R)$ is found with a certain probability p_u is calculated by

finding the value l_u that defines the interval $(0, l_u)$ in which the random variable $l(R)$ given by Eq. (14) is found with probability p_u . The probability p_u is calculated as the integral of the joint probability density function of $\eta(R)$ and $\zeta(R)$ over the shadowed area in Fig. 1, limited by the lines

$$\frac{1 + \eta(R)}{1 + \zeta(R)} = 1, \quad \frac{1 + \eta(R)}{1 + \zeta(R)} = 1 + l_u. \quad (15)$$

Under the approximation represented by Eq. (10), $\zeta_m(R)$ and $\zeta_i(R)$ can be considered uncorrelated, because the weight of any random variable $n(z)dz$ in the integral in Eq. (8) is infinitesimally small. From a physical point of view this approximation means that we consider negligible the effect of the noise in a resolution cell as compared to the linear combination of noises in many other resolution cells. We will assume in addition henceforth that $n(R)$ is a Gaussian stochastic process to a good degree of approximation. Actually the noise sources of a photoreceiver can be broadly classified into shot noise and thermal noise. Thermal noise can be represented by a Gaussian process, and, if the rate r_s (photons/s or charge carriers/s) of a shot-noise source is high enough compared to the system bandwidth B , shot noise can also be approximated by a Gaussian process [25]. We will assume that the shot-noise sources, including the flow of incoming photons, satisfy this condition. Hence the random variables $\zeta_m(R)$ and $\zeta_i(R)$ follow a joint Gaussian law because they are obtained as the result of applying linear operators to the basic Gaussian process $n(R)$ [26], and their sum $\zeta(R)$ is also a Gaussian random variable. Its standard deviation is $\sigma_\zeta = \sqrt{\sigma_{\zeta_i}^2(R) + \sigma_{\zeta_m}^2(R)}$, and its mean is zero because $\zeta_m(R)$ and $\zeta_i(R)$ are uncorrelated zero mean.

For similar reasons, $\eta(R)$ and $\zeta(R)$ can be treated as uncorrelated, zero-mean random (except in the particular but virtually irrelevant case that $R = R_m$) and jointly Gaussian variables. Since they are uncorrelated, their joint probability density function is given by

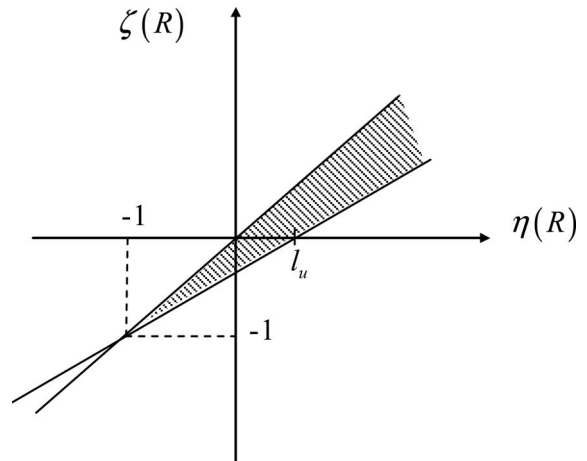


Fig. 1. Integration domain for calculating p_u .

$$f_{\eta\zeta}(\eta, \zeta) = \frac{1}{2\pi\sigma_\eta\sigma_\zeta} \exp\left(-\frac{\eta^2}{2\sigma_\eta^2}\right) \exp\left(-\frac{\zeta^2}{2\sigma_\zeta^2}\right). \quad (16)$$

According to the standard deviation values discussed in Subsection 3.B, $\sigma_\eta = \sigma_n(R)/P(R)$ (the explicit dependence on R of σ_η is dropped in the notation for simplicity). The probability p_u is then given by

$$p_u = \frac{1}{2\pi\sigma_\eta\sigma_\zeta} \int_{-1}^{\infty} \exp\left(-\frac{\zeta^2}{2\sigma_\zeta^2}\right) \int_{\zeta}^{\zeta(1+l_u)+l_u} \times \exp\left(-\frac{\eta^2}{2\sigma_\eta^2}\right) d\eta d\zeta, \quad (17)$$

which can also be written as

$$p_u = \frac{1}{2\sqrt{2}\pi\sigma_\zeta} \int_{-1}^{\infty} \exp\left(-\frac{\zeta^2}{2\sigma_\zeta^2}\right) \left\{ \operatorname{erf}\left[\frac{\zeta(1+l_u)+l_u}{\sqrt{2}\sigma_\eta}\right] - \operatorname{erf}\left[\frac{\zeta}{\sqrt{2}\sigma_\eta}\right] \right\} d\zeta. \quad (18)$$

Given a value, Eq. (18) can be solved for the corresponding l_u value.

Likewise it can be shown that the interval $(\beta_a(R) - l_l\beta(R), \beta_a(R))$ in which $\hat{\beta}_a$ lies with probability p_l is found by solving for l_l the equation

$$p_l = \frac{1}{2\sqrt{2}\pi\sigma_\zeta} \int_{-1}^{\infty} \exp\left(-\frac{\zeta^2}{2\sigma_\zeta^2}\right) \left\{ \operatorname{erf}\left(\frac{\zeta}{\sqrt{2}\sigma_\eta}\right) - \operatorname{erf}\left[\frac{\zeta(1-l_l)-l_l}{\sqrt{2}\sigma_\eta}\right] \right\} d\zeta. \quad (19)$$

It can be shown that if $\sigma_\zeta \ll 1$ and $l_u \ll 1, l_l \ll 1$, then $p_u \approx \frac{1}{2} \operatorname{erf}[l_u/\sqrt{2(\sigma_\eta^2 + \sigma_\zeta^2)}]$ and $p_l \approx \frac{1}{2} \operatorname{erf}[l_l/\sqrt{2(\sigma_\eta^2 + \sigma_\zeta^2)}]$, in agreement with the classical (perturbational) error propagation method, in which assuming a small value of σ_ζ we would have approximated $(1 + \eta)/(1 + \zeta) \approx 1 + \eta - \zeta$.

4. Example

The error limits resulting from the calculation of the standard deviations of $\eta(R)$ and $\zeta(R)$ in the case of the two-component algorithm are illustrated by using the same input data as in Ref. [24]. The photoreceiver electrical bandwidth was 10 MHz, and the output was digitized at $B = 20$ megasamples/s (hence $\Delta\tau = \frac{1}{2B}$), yielding a range resolution $\Delta R = 7.5$ m. Other technical details about the instrument used can be found in Ref. [24]. The lidar profile was acquired at the wavelength of 1064 nm. Figure 2 shows the noise-contaminated lidar range-corrected signal between 600 and 6180 m. Several aerosol layers are clearly observed until 4900 m approximately; we assume that the atmosphere is purely molecular above that distance. As in the last figure of Ref. [24], we explored two cases depending on the number of resolution cells, N , used to average the values of $\hat{P}(R)$ around R_m and to force $\hat{P}(R_m)$ to this

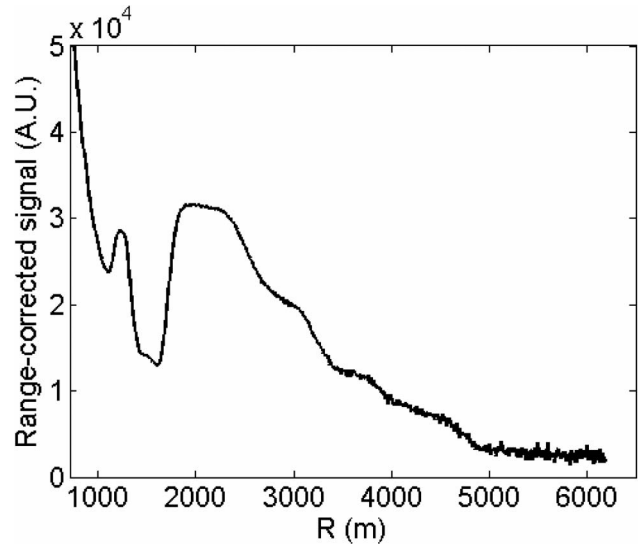


Fig. 2. Lidar range-corrected signal between 600 and 6180 m for 4000 pulses integrated at 1064 nm.

average value: $N = 1$ (no average) and $N = 17$ (average between $R_m - 60$ and $R_m + 60$ m). A constant aerosol lidar ratio value of $S_a = 50$ sr was used to perform the inversion, and β_m was taken according to the molecular atmosphere model proposed in Ref. [27] for the 1064 nm wavelength under standard conditions of pressure and temperature. Note however that we are not emphasizing the physical characteristics of the atmosphere for this particular case—whether the aerosol lidar ratio accurately corresponds to the actual situation or if corrections to β_m should be made to take into account departures of the actual atmospheric conditions from the standard ones—but rather the mathematical aspects of the effect of noise on the inversion. In this respect, note also that although a constant lidar ratio is used in the example, the formulation allows for a function with an arbitrary dependence on range that could be employed if by some means information on the lidar ratio is available.

The standard deviations of η , ζ_m , and ζ_i — σ_η , σ_{ζ_m} , and σ_{ζ_i} —are represented in Fig. 3. Note that the number of cells N only affects σ_{ζ_m} . As the range decreases, the signal-to-noise ratio increases, therefore σ_η decreases, as shown in the figure. Instead, by averaging over $N = 17$ cells around R_m , σ_{ζ_m} decreases by a factor of 4 to 5 compared to the initial value when no average is performed ($N = 1$), to a value around 0.05. In that case, the approximation $\sigma_{\zeta_m} \ll 1$ can be made as Fig. 4 also shows. As expected, the term σ_{ζ_i} is very small compared to the other two standard deviations.

Figure 4 shows the aerosol backscatter coefficient and its error bounds in a 68% confidence interval found by setting $p_u = p_l = 34\%$ (to maintain a common criterion with the probability of one standard deviation of a Gaussian probability law below and above the “true” value, usually employed to define error bars in classical error-propagation approaches) for $N = 1$ (Fig. 4(a)) and $N = 17$ (Fig. 4(b)). The “true”

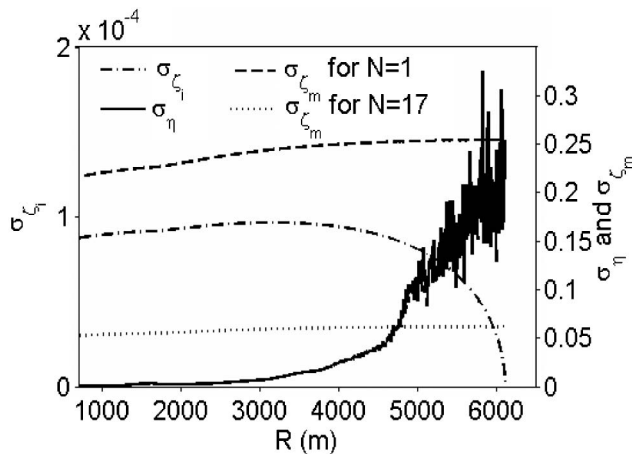


Fig. 3. Standard deviations, σ_η , σ_{ζ_m} , and σ_{ζ_i} , of η (solid curve), ζ_m (dashed and dotted curves), and ζ_i (dash-dotted curve), respectively. The axes legend of σ_{ζ_i} (dash-dotted curve) is on the left side of the figure. The axes legends of σ_η and σ_{ζ_m} are on the right side of the figure.

value has been taken as the central profile in the family of 17 profiles obtained when the inversion starting range is varied from 6000 to 6120 m with $N = 17$. In Fig. 4(a) the asymmetrical behavior of the error bounds is clearly visible, because the value of σ_ζ for $N = 1$ varies around 0.25, which cannot be considered small compared to 1. However, when $N = 17$ (Fig. 4(b)) the upper and lower error bounds are almost perfectly symmetric, since $\sigma_\zeta \approx 0.05 \ll 1$, and classical error propagation is justified. In the case presented here, the error bars on the aerosol backscatter coefficient are lower than 15% below 5000 m and lower than 7% below 4000 m, where the signal-to-noise ratio is around 11 and 42, respectively. When averaging the values of $P(R)$ around R_m to reduce the effect of noise in the cell from which the inversion is started, the effective value of σ_{nm} is divided by \sqrt{N} . However, when proceeding in this manner one cannot indefinitely increase N to decrease σ_{nm} as the maximum allowable number of averaged cells is limited by the dependence on R of the received power being well approximated by a linear law through the range covered by the N cells [24]. In practice the linear approximation will be safely satisfied if $N\Delta R$ does not exceed a few hundreds of meters. More sophisticated approaches, like adjusting a theoretical molecular backscatter profile to the measured one, can be used to filter out noise affecting the starting cell [28].

5. Conclusions

Expressions have been derived for the calculation of statistical error bounds for the aerosol backscatter coefficient retrieved by the two-component lidar inversion method. The expressions depend on the signal-to-noise ratio along the inversion path and take into account “instantaneous” effects (the effect of the signal-to-noise ratio at the range where the aerosol backscatter coefficient is being computed) as well as “memory” effects, namely, both the effect

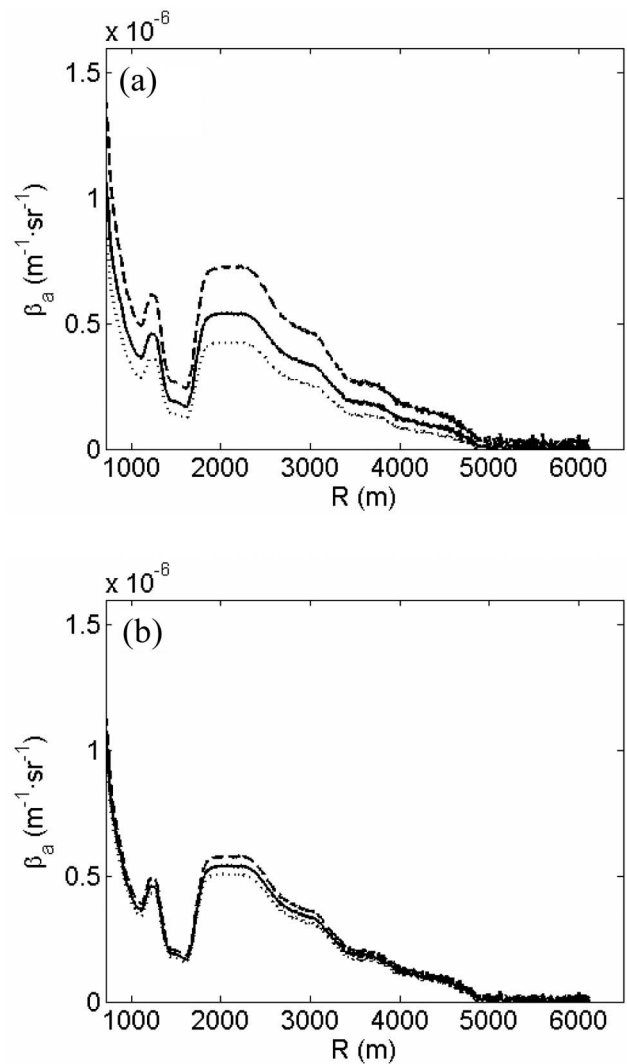


Fig. 4. Lower (dotted curve) and upper (dashed curve) estimated 68% confidence interval for the inverted backscatter coefficient: (a) $N = 1$ and (b) $N = 17$ [$R_m - 60, R_m + 60$ m].

of the signal-to-noise ratio in the cell where the inversion is started and the cumulative effect of the noise between that cell and the actual cell where the aerosol backscatter coefficient is evaluated. The standard deviations of the random variables representing these effects allow assessment of their relative importance. The utilization of these expressions has been illustrated with an example on real lidar data. Although the example presented has been done on the two-component algorithm (backward) and on data obtained from a ground-based, upward looking lidar, the formulation developed in this paper is also valid for the forward solution of the elastic lidar inversion and for any line of sight. They are also valid for signal-to-noise ratio situations in which a perturbational classical error propagation approach would not be valid (although they reduce to error propagation results for low enough standard deviations of the noise terms). It has been shown how the effect of the signal-to-noise ratio at the range where the inversion is started can be reduced by averaging the

noise-contaminated signal over a number of cells around that range.

The method presented in this paper permits assessment in a quantitative manner the statistical error produced on the retrieved aerosol backscatter coefficient when inverting noise-corrupted lidar signals. With the quasi-analytical formulas supplied in this paper, the calculation of the error produced on the aerosol backscatter coefficient retrieval from noise-corrupted lidar signals only requires a simple program dedicated mainly to solve Eqs. (18) and (19).

The work presented here was supported by the European Union and FEDER funds under the EARLINET-ASOS project (EU Coordination Action, contract 025991 (RICA)); by the European Space Agency under the project 21487/08/NL/HE; and by the MICINN (Spanish Ministry of Science and Innovation) and FEDER funds under the project TEC2006-07850/TCM, and the Complementary Actions CGL20007-28871-E/CLI, CGL2006-26149-E/CLI, and CGL2008-01330-E/CLI. M. Sicard is grateful to the MICINN for the Ramón y Cajal position he holds. Finally, the authors wish to thank both referees for the historical insights they provided to reference properly the elastic, single wavelength lidar inversion methods.

References

1. P. Forster, V. Ramaswamy, P. Artaxo, T. Bernsten, R. Betts, D. W. Fahey, J. Haywood, J. Lean, D. C. Lowe, G. Myhre, J. Nganga, R. Prinn, G. Raga, M. Schulz, and R. Van Dorland, "Changes in atmospheric constituents and in radiative forcing," in *Climate Change 2007: The Physical Science Basis. Contribution of Working Group I to the Fourth Assessment Report of the Intergovernmental Panel on Climate Change*, S. Solomon, D. Qin, M. Manning, Z. Chen, M. Marquis, K. B. Averyt, M. Tignor, and H. L. Miller, eds. (Cambridge Univ. Press, 2007), pp. 129–234.
2. J. Bösenberg, A. Ansmann, J. M. Baldasano, D. Balis, C. Böckmann, B. Calpini, A. Chaikovskiy, P. Flamant, A. Hågård, V. Mitev, A. Papayannis, J. Pelon, D. Resendes, J. Schneider, N. Spinelli, T. Trickl, G. Vaughan, G. Visconti, and M. Wiegner, "EARLINET: A European aerosol research lidar network," in *Advances in Laser Remote Sensing of the Atmosphere*, A. Dabas, C. Loth, and J. Pelon, eds. (Edition Ecole Polytechnique, 2001), pp. 155–158.
3. E. J. Welton, J. R. Campbell, J. D. Spinhirne, and V. S. Scott, "Global monitoring of clouds and aerosols using a network of micro-pulse lidar systems," *Proc. SPIE* **4153**, 151–158 (2001).
4. R. Hoff, G. Pappalardo, and J. Bösenberg, "GAW Aerosol Lidar Observations Network (GALION)," paper presented at the Symposium on Recent Developments in Atmospheric Applications of Radar and Lidar of the 88th annual meeting of the American Meteorological Society, New Orleans, Louisiana, US, 20–24 July 2008.
5. D. Winker, J. Pelon, and M. McCormick, "Initial results from CALIPSO," in *Reviewed and Revised Papers Presented at the 23rd International Laser Radar Conference*, C. Nagasawa and N. Sugimoto, eds. (Tokyo Metropolitan Univ., 2006), pp. 991–994.
6. D. Winker, W. Hunt, and M. McGill, "Initial performance assessment of CALIOP," *Geophys. Res. Lett.* **34**, L19803 (2007).
7. P. Dubock, M. Endmann, and P. Ingmann, "Progress with ADM-Aeolus, the Spaceborne Doppler Wind Lidar ADM," in *Reviewed and Revised Papers Presented at the 23rd International Laser Radar Conference*, C. Nagasawa and N. Sugimoto, eds. (Tokyo Metropolitan Univ., 2006), pp. 1011–1014.
8. A. Hélière, J. L. Vézy, A. Lefebvre, W. Leibbrandt, C. C. Lin, T. Wehr, T. Kimura, and H. Kumagai, "The ESA EarthCARE Mission: mission concept and lidar instrument pre-development," in *Reviewed and Revised Papers Presented at the 23rd International Laser Radar Conference*, C. Nagasawa and N. Sugimoto, eds. (Tokyo Metropolitan Univ., 2006), pp. 1041–1044.
9. F. G. Fernald, B. M. Herman, and J. A. Reagan, "Determination of aerosol height distribution by lidar," *J. Appl. Meteorol.* **11**, 482–489 (1972).
10. F. G. Fernald, "Comments on the analysis of atmospheric lidar observations," in *Proceedings of the 11th International Laser Radar Conference*, NASA Conf. Publ. 2228, 213–215 (1982).
11. F. G. Fernald, "Analysis of atmospheric lidar observations: some comments," *Appl. Opt.* **23**, 652–653 (1984).
12. E. W. Barrett and O. Ben-Dov, "Application of the lidar to air pollution measurements," *J. Appl. Meteorol.* **6**, 500–515 (1967).
13. W. Viezee, E. E. Uthe, and R. T. H. Collis, "Lidar observations of airfield approach conditions: an exploratory study," *J. Appl. Meteorol.* **8**, 274–283 (1969).
14. P. A. Davis, "The analysis of lidar signatures of cirrus clouds," *Appl. Opt.* **8**, 2099–2102 (1969).
15. W. Hitschfeld and J. Bordan, "Errors inherent in the radar measurement of rainfall at attenuating wavelengths," *J. Atmos. Sci.* **11**, 58–67 (1954).
16. J. D. Klett, "Stable analytical inversion solution for processing lidar returns," *Appl. Opt.* **20**, 211–220 (1981).
17. Y. Sasano and H. Nakane, "Significance of the extinction/backscatter ratio and the boundary value term in the solution for the two-component lidar equation," *Appl. Opt.* **23**, 11–13 (1984).
18. Q. Jinhuan, "Sensitivity of lidar equation solution to boundary values and determination of the values," *Adv. Atmos. Sci.* **5**, 229–241 (1988).
19. M. Matsumoto and N. Takeuchi, "Effects of misestimated far-end boundary values on two common lidar inversion solutions," *Appl. Opt.* **33**, 6451–6456 (1994).
20. L. R. Bissonnette, "Sensitivity analysis of lidar inversion algorithms," *Appl. Opt.* **25**, 2122–2125 (1986).
21. F. Rocadenbosch and A. Comerón, "Error analysis for the lidar backward inversion algorithm," *Appl. Opt.* **38**, 4461–4474 (1999).
22. H. G. Hughes, J. A. Ferguson, and D. H. Stephens, "Sensitivity of a lidar inversion algorithm to parameters relating atmospheric backscatter and extinction," *Appl. Opt.* **24**, 1609–1613 (1985).
23. Y. Sasano, E. V. Browell, and S. Ismail, "Error caused by using a constant extinction/backscattering ratio in the lidar solution," *Appl. Opt.* **24**, 3929–3932 (1985).
24. A. Comerón, F. Rocadenbosch, M. A. López, A. Rodríguez, C. Muñoz, D. García-Vizcaíno, and M. Sicard, "Effects of noise on lidar data inversion with the backward algorithm," *Appl. Opt.* **43**, 2572–2577 (2004).
25. A. Papoulis, *Probability, Random Variables and Stochastic Processes*, (McGraw-Hill, 1965), Sect. 16–5.
26. A. Papoulis, *Probability, Random Variables and Stochastic Processes*, (McGraw-Hill, 1965), Sect. 8.4.
27. B. A. Bodhaine, N. B. Wood, E. G. Dutton, and J. R. Slusser, "On Rayleigh optical depth calculations," *J. Atmos. Ocean Technol.* **16**, 1854–1861 (1999).
28. T. Trickl, Forschungszentrum Karlsruhe, Institut für Meteorologie und Klimaforschung (IMK-IFU), Kreuzteckbahnstrasse 19, D-82467 Garmisch-Partenkirchen, Germany, private communication, 1 October 2008.